COBEM 2023 27TH INTERNATIONAL CONGRESS OF MECHANICAL ENGENEERING

ABCM Brazilian Society of Mechanical Sciences and Engineering
27th ABCM International Congress of Mechanical Engineering
December 04-08, 2023, Florianópolis-SC, Brazil

COB-2023-0810
A POSITIONAL FEM FORMULATION FOR GEOMETRICALLY NONLINEAR ANALYSIS OF LAMINATED PLATES AND SHELLS: REGULARIZATION OF TRANSVERSE NORMAL AND SHEAR STRESSES

Vinícius de Barros Souza
Humberto Breves Coda
Dept. of Structural Engineering, São Carlos School of Engineering, University of São Paulo
Av. Trab. São Carlense, 400, 13566-590, São Carlos, São Paulo, Brazil
vbarros@usp.br; hbcoda@sc.usp.br

Abstract. *Composite materials and structures have drawn special attention in the technical and scientific community due to their vast applications in areas of engineering, especially in civil, aeronautics, and aerospace industries. However, the distribution of transverse stresses along the laminate thickness is complex and a few theories can determine it accurately. The present study exploits the mechanical behavior of geometrically nonlinear laminated plates and shells applying an alternative formulation of the Finite Element Method (FEM). The so-called positional FEM is a geometrically exact and Total Lagrangian formulation that uses generalized vectors and nodal positions as parameters. A ten-node degenerate shell finite element with six degrees of freedom per node is employed in the basic kinematics, in which two enrichments are introduced. The first one promotes a linear strain variation along the thickness to mitigate volumetric locking of the cross section. The second introduces two new degrees of freedom in the composite's reference surface directions, related with the regularization of transverse stresses and the intensity of the zigzag displacement field. According to the results, the proposed kinematics can simulate the shear and normal stresses fields, satisfying the continuity of shear stresses regarding transverse direction. In addition, the formulation has proved to be stable in strongly nonlinear analyses and free of volumetric locking.*

Keywords: *stress distribution, laminated plates and shells, orthotropic material, nonlinear analysis, positional FEM*

1. INTRODUCTION

Laminated composite structures and materials are formed by stacking layers of different material properties seeking a final product with physical, chemical, and/or mechanical properties superior to those of its individual components. Examples are sandwich panels and fiber-reinforced structures oriented in different directions. The wide applications of the laminated structures, especially in the engineering fields, have stimulated great interests in development of sufficiently accurate mathematical models to predict their mechanical behavior, particularly stress distribution and failure mechanisms triggered by interlaminar stresses (Wu *et al.*, 2018; Liew *et al.*, 2019).

The transverse anisotropy associated with the geometric properties of the laminated structure can provides a complex behavior involving abrupt slope in the displacement field along adjacent interfaces, the so-called zigzag pattern (Carrera, 2003; Garg and Chalak, 2019; Li, 2021). In the last half century, many theories have been proposed for the analysis of composite structures, generally grouped into three categories (Tornabene, 2016): the three-dimensional elasticity (3D), the equivalent single-layer theories (ESL) and the layer-wise theories (LW). The former treats the laminated structure as a general 3D solid, providing accurate results. The first analytical solutions for laminated structures were obtained by Pagano (1969, 1970) within 3D elasticity, and have been used still nowadays as a benchmark for validation of transverse stresses (Vu-Quoc and Tan, 2013; Coda *et al.*, 2022; Sorrenti and Gherlone, 2023). However, these solutions are limited to particular cases. More generalized results can be obtained numerically, although 3D theories are highly computationally expensive (Liew *et al.*, 2019).

In the ESLs, as the own name suggests, the layered structure is modelled as a single layer with homogenized properties (Petrolo *et al.*, 2023). These theories are derived from the 3D elasticity through assumptions concerning the kinematics of deformation or the stress state in the thickness direction, which allow the reduction of 3D problems into two-dimensional problems (Reddy, 2004). It is well known that ESL theories can provide good results for the global responses, but they are not enough to satisfy piecewise continuous displacement and to represent transverse stress fields accurately. The ESLs include the classical laminated theory (CLT), first-order shear deformation theories (FSDT), and higher-order shear deformation theories (HSDT), in which the first two are the most widely used in composite structure analyses (Liew *et al.*, 2019; Li, 2021). According to Reddy (2004), although more accurate, the HSDT theories are intended for particular cases,

as the resulting high-order stresses are difficult to interpret physically.

On the other side, LW theories treats each layer independently as a 3D solid, employing full 3D kinematics and constitutive relations, and continuous functions (class C_0) for the displacement field at the layer interface. Since they are able to provide results comparable to 3D elasticity solutions, LW approaches are widespread in the literature (Reddy, 2004; Tornabene, 2016; Soltani and Kordkheili, 2021). However, LW theories can require high computational effort depending on the number of layers.

This study applies a subclass of LW model, namely zigzag theory (Icardi, 2001; Carrera, 2003; Tessler *et al.*, 2009), in which the displacement field is a superposition of the global displacement and a local zigzag function per layer, linear or higher order. By imposing the interlaminar continuity of transverse stresses, the number of unknowns become independent of the number of layers (Wanji and Zhen, 2008), which is a computational advantage regarding the classical LW theories.

The basic kinematics used herein is Reissner-Mindlin-like. To overcome inherent limitations of this theory, two enrichments are proposed: a linear strain in the thickness and linear zigzag displacements functions in the directions of the composite's reference surface. The latter introduces the regularization of shear stresses related with the basic kinematics and the intensity of the zigzag pattern, providing continuous shear stress distribution through the thickness. These enhancements are carried out analytically for small displacements and strains equations using a beam framework, although they are extended to plate and shell large displacement applications thanks to a scaling strategy.

The numerical results are provided by the positional FEM formulation (Bonet *et al.*, 2000; Coda and Paccola, 2007). In the mechanical model, this formulation uses Green-Lagrange strain, Second Piola-Kirchhoff stress, and Saint-Venant-Kirchhoff constitutive law for isotropic or orthotropic materials. However, for comparison reasons, the Cauchy stress is post-processed. To obtain the equation of motion, the study applies the total mechanical energy stationary principle regarding positions. Furthermore, the numerical framework uses the Newton-Raphson method to solve the system of nonlinear equations, while the Newmark algorithm performs temporal integration in transient dynamic analysis.

The positional formulation and proposed enrichments are presented in Section 2, in addition to the basic kinematics. Section 3 presents two numerical applications. The results shows the excellent performance of the positional FEM in problems developing large displacements, including the zigzag pattern in laminated composite. The accuracy to predict the distribution of transverse stresses in symmetrical laminated composites is evaluated in subsection 3.2 through a comparison with classical elasticity solutions.

2. THE POSITIONAL FINITE ELEMENT METHOD

The positional FEM, originally conceived by Bonet *et al.* (2000) for fluid-supported membrane analysis and later extended by Coda (2003) for solid mechanics applications, uses nodal positions and generalized vectors as nodal parameters when dealing with plates and shells. The approach presented in this section is based on Coda (2018), whose reference is recommended for further details.

This study uses a triangular degenerate shell element with cubic approximation order. The finite element discretization is performed on the reference surface of the plate or shell, while the initial thickness (h_0) is constant and introduced as a geometric property.

2.1 Basic kinematics

The basic kinematics is described by the mapping functions f_i^0 and f_i^1, which provide the initial (x_i) and current (y_i) coordinates of the continuum, respectively, where index i represents the vector component associated with the finite element node. Considering the shell's (or plate) reference surface in the stiffness center of the cross section, the mapping functions at initial and current configurations are, respectively:

$$f_i^{0\,k}(\xi_1,\xi_2,\xi_3) = x_i^k = \phi_i^\alpha(\xi_1,\xi_2)X_i^\alpha \;+\; z_k(\xi_3)\phi_z(\xi_1,\xi_2)V_i^z, \tag{1}$$

$$f_i^{1\,k}(\xi_1,\xi_2,\xi_3) = y_i^k = \phi_i^\alpha(\xi_1,\xi_2)Y_i^\alpha \;+\; z_k(\xi_3)\phi_z(\xi_1,\xi_2)G_i^z, \tag{2}$$

where $z_k(\xi_3) = d^k + (h_0^k/2)\xi_3$, in which k represents a layer of thickness h_0^k, and d^k the distance from the reference surface of layer k to the reference surface. X_i^α and Y_i^α are the i-th initial and current coordinates of node α, respectively. $\vec{V}$ is the generalized vector in the initial configuration (unitary and normal to the reference surface) and $\vec{G}$ is the generalized vector in the current configuration (without restrictions). The Lagrangian shape functions ϕ_α associated with nodes α are written in dimensionless coordinates ξ_1 and ξ_2 at the reference surface. The isoparametric domain is completed with ξ_3, a dimensionless coordinate that generates the thickness direction.

Using Eq. (1) and Eq. (2), the change of configuration function $\vec{f}$ is written, for a given layer k, as:

$$\vec{f}^{\,k} = \vec{f}^{\,1\,k} \circ (\vec{f}^{\,0\,k})^{-1}, \tag{3}$$

and its gradient matrix $\mathbf{A}$ is given by:

$$\mathbf{A}^k = \nabla(\vec{f}^{\,k}) = \mathbf{A}^{1\,k} \cdot (\mathbf{A}^{0\,k})^{-1}, \tag{4}$$

where:

$$A_{ij}^{0\,k} = \frac{\partial f_i^{0\,k}}{\partial \xi_j} \quad \text{and} \quad A_{ij}^{1\,k} = \frac{\partial f_i^{1\,k}}{\partial \xi_j} \quad (i,j = 1,2,3). \tag{5}$$

Therefore, the basic kinematics comprises six known nodal parameters in the initial configuration, stored in vector $\vec{X} = \{X_1, X_2, X_3, V_1, V_2, V_3\}^t$, and six unknown degrees of freedom per node in the current configuration ($\vec{Y} = \{Y_1, Y_2, Y_3, G_1, G_2, G_3\}^t$). To orthotropic material, this vectors are transformed to the orthotropic direction as follows:

$$\vec{\bar{X}} = \mathbf{R}^t \cdot \vec{X} \quad \text{and} \quad \vec{\bar{Y}} = \mathbf{R}^t \cdot \vec{Y}, \tag{6}$$

where $\mathbf{R}$ is the rotation matrix, and $\vec{\bar{X}}$ and $\vec{\bar{Y}}$ are the parameters vectors in the local direction.

2.2 Kinematics enrichments

Seeking a quadratic variation of the thickness in the current configuration, an enrichment is introduced in the basic kinematics through nodal parameter T, thus avoiding the "thickness locking", as described by Bischoff and Ramm (1997). The second enrichment introduces the zigzag mode $a_{ik}z_k + b_{ik}$ in the directions of the reference surface ($i = 1, 2$), where $z_k = z_k(\xi_3)$, and a_{ik} and b_{ik} are constants of straight lines for the k-th layer. These constants are determined only once for each cross section by imposing compatibility and equilibrium conditions between contiguous layers (Coda *et al.*, 2022).

The proposed enrichments are introduced in the $\vec{f}^1$ mapping function, presented in Eq. (2). For symmetrically laminated plates and shells, one writes:

$$\begin{aligned} f_i^{1\,k}(\xi_1,\xi_2,\xi_3) = \phi_\alpha(\xi_1,\xi_2)Y_i^\alpha + \left[z_k + z_k^2\phi_\gamma T_\gamma\right]\phi_z(\xi_1,\xi_2)G_i^z + \phi_m(\xi_1,\xi_2)Z_m^1\left[a_{1k}z_k + b_{1k}\right]\phi_j(\xi_1,\xi_2)\bar{G}_i^{1j} + \\ + \phi_n(\xi_1,\xi_2)Z_n^2\left[a_{2k}z_k + b_{2k}\right]\phi_p(\xi_1,\xi_2)\bar{G}_i^{2p}, \end{aligned} \tag{7}$$

where Z_α^i is a new degree of freedom (intensity of the zigzag mode) at node α following direction i. Furthemore, $\vec{\bar{G}}^1$ and $\vec{\bar{G}}^2$ are vectors orthogonal to the generalized ones at directions 1 and 2, respectively.

In order to smooth the stress distribution, the following deductions are described for a horizontal beam developing small displacements (with rotation θ and axial points displacements d_1):

$$d_1^k = \phi_\alpha(\xi_1)U_1^\alpha + z_k\phi_i(\xi_1)\theta_i + \phi_j(\xi_1)Z_j(a_k z_k + b_k), \tag{8}$$

in which $U_1^\alpha = Y_1^\alpha - X_1^\alpha$.

By sectioning the beam longitudinally, the equilibrium of forces orthogonal to the cross section provides:

$$\tau^k = \int_{z_k}^{z^{top}} \frac{\partial \sigma_{11}^k}{\partial x_1}\, dz, \tag{9}$$

where z^{top} is the upper limit of the cross section, and σ_{11} is the normal stress. According to Hooke's law of elasticity:

$$\sigma_{11}^k = E_k \frac{\partial d_1^k}{\partial x_1}, \tag{10}$$

in which E_k is the longitudinal Young modulus of layer k.

Neglecting the portion related to the normal force ($\phi_\alpha U_1^\alpha$) in Eq. (8), one writes:

$$\sigma_{11}^k = E_k z_k \phi_i'(\xi_1)\theta_i + E_k\phi_j'(\xi_1)Z_j(a_k z_k + b_k), \tag{11}$$

$$\frac{\partial \sigma_{11}^k}{\partial x_1} = E_k z_k \phi_i''(\xi_1)\theta_i + E_k\phi_j''(\xi_1)Z_j(a_k z_k + b_k), \tag{12}$$

where primes represent derivatives with respect to x_1.

Replacing Eq. (12) in Eq. (9), the shear stress τ in the horizontal beam developing small displacements is:

$$\tau^k = \int_{z_k}^{z^{top}} \left[E_k z_k \phi_i^{''}\theta_i + E_k\phi_j^{''}Z_j(a_k z_k + b_k)\right] dz. \tag{13}$$

Solving Eq. (13) and dividing the result by the shear elastic modulus of layer k (G^k), one provides the distortion γ^k:

$$\gamma^k = \left[A_k + C_k(z_k^{top})^2 - C_k z_k^2\right]\phi_j^{''}(\xi)\theta_j + \left\{F_k + I_k\left[(z_k^{top})^2 - z_k^2\right] + L_k + M_k(z_k^{top} - z_k)\right\}\phi_p^{''}Z_p, \tag{14}$$

whose constants are:

$$A_k = \frac{1}{G^k}\sum_{i=k+1}^{n} E_i \bar{z}_i h_0^i, \quad F_k = \frac{1}{G^k}\sum_{i=k+1}^{n} E_i a_i \bar{z}_i h_0^i, \quad L_k = \frac{1}{G^k}\sum_{i=k+1}^{n} E_i b_i h_0^i, \quad C_k = \frac{E_k}{2G^k}, \\ I_k = \frac{E_k a_k}{2G^k}, \quad M_k = \frac{E_k b_k}{G^k}, \tag{15}$$

in which $\bar{z}$ is the distance from the stiffness center to the midline of the layer.

The integration of Eq. (14) along the cross section yields the horizontal displacement profile $\bar{d}_1$, in which the upper bar indicates a scaling to be introduced. The scale strategy is presented in Coda *et al.* (2022), where the following expression can be written for small displacements:

$$d_1^k = \phi_\alpha(\xi_1,\xi_2)U_1^\alpha + u_1^k(z)\phi_i(\xi_1,\xi_2)\theta_i + u_2^k(z)\phi_j(\xi_1,\xi_2)Z_j, \tag{16}$$

where:

$$u_1^k(z) = A_k z + C_k\left[(z_k^{top})^2 - \frac{z^2}{3}\right]z, \tag{17}$$

$$u_2^k(z) = (F_k + L_k)z + I_k\left[(z_k^{top})^2 - \frac{z^2}{3}\right]z + M_k\left(z_k^{top} - \frac{z}{2}\right)z. \tag{18}$$

Towards the introduction of Eq. (16) in the geometrically nonlinear formulation, z_k is subtracted from u_1^k in order to preserve rigid body movements. This is performed in both directions orthogonal to the thickness by introducing the term $r_i^k = u_1^{ik} - z_k$, which generates the new degree of freedom R_α^i at node α for $i = 1, 2$. From this considerations, Eq. (7) is rewritten as:

$$f_i^{1\,k}(\xi_1,\xi_2,\xi_3) = \phi_\alpha(\xi_1,\xi_2)Y_i^\alpha + \left[z_k + z_k^2\phi_\gamma(\xi_1,\xi_2)T_\gamma\right]\phi_z(\xi_1,\xi_2)G_i^z + \\ + \left[r_1^k(\xi_3)\phi_m(\xi_1,\xi_2)R_m^1 + u_2^{1k}(\xi_3)\phi_s(\xi_1,\xi_2)Z_s^1\right]\phi_j(\xi_1,\xi_2)\bar{G}_i^{1j} + \\ + \left[r_2^k(\xi_3)\phi_n(\xi_1,\xi_2)R_n^2 + u_2^{2k}(\xi_3)\phi_l(\xi_1,\xi_2)Z_l^2\right]\phi_p(\xi_1,\xi_2)\bar{G}_i^{2p}. \tag{19}$$

Therefore, the introduction of R_α^i and Z_α^i in the f^1 mapping function leads to a kinematics with 11 degrees of freedom per node.

2.3 Equilibrium equations and numerical solution

The equation of motion in the positional FEM is based on the Principle of Stationary Mechanical Energy, i.e., the first variation of the total mechanical energy (Π) regarding positions is null. The functional of energy Π is composed of three terms: potential energy of external forces ($\mathbb{P}$), total strain energy ($\mathbb{U}$), and kinetic energy ($\mathbb{K}$). Therefore, the principle is written as:

$$\delta\Pi = \frac{\partial\Pi}{\partial\vec{Y}}\delta\vec{Y} = \left(\frac{\partial\mathbb{U}}{\partial\vec{Y}} + \frac{\partial\mathbb{P}}{\partial\vec{Y}} + \frac{\partial\mathbb{K}}{\partial\vec{Y}}\right)\delta\vec{Y} = \vec{0}, \tag{20}$$

where $\delta\vec{Y}$ is the variation of position (arbitrary), and:

$$\frac{\partial\mathbb{U}}{\partial\vec{Y}} = \int_{V_0}\mathbf{S} : \frac{\partial\mathbf{E}}{\partial\vec{Y}}dV_0, \tag{21}$$

$$\frac{\partial\mathbb{P}}{\partial\vec{Y}} = -\int_{A_0} q_{i\alpha}^0\phi_\alpha(\xi_1,\xi_2)\phi_\gamma(\xi_1,\xi_2)dA_0, \tag{22}$$

$$\frac{\partial\mathbb{K}}{\partial\vec{Y}} = h_0\int_{A_0}\rho_0\ddot{y}_i dA_0, \tag{23}$$

in which $\mathbf{S} = \mathfrak{C} : \mathbf{E}$ is the second Piola-Kirchhoff stress tensor, $\mathbf{E}$ is the Green-Lagrange strain tensor, $\mathfrak{C}$ is the elastic constitutive tensor (Saint-Venant-Kirchhoff). Furthermore, $q_{i\alpha}^0$ is the distributed surface conservative load written as a function of nodes α and direction i, ρ_0 is the material density, $\ddot{y}_i$ is the acceleration, A_0 is the reference surface area, V_0 is the plate or shell volume, and index 0 indicates the Lagrangian description of the formulation.

The system of equations obtained from Eq. (20) is nonlinear regarding nodal parameters ($\vec{Y}$). The strategy adopted to solve this system is the Newton-Raphson iterative method. In general terms, the Newton-Raphson procedure involves the choice of a trial solution $\vec{Y_0}$, and calculation of residuum vector $\vec{g}(\vec{Y_0})$ by Eq. (24). From the Hessian matrix $\mathbf{H}$ of the

problem, Eq. (25) provides the correction $\Delta\vec{Y}$ imposed on the trial position $\vec{Y_0}$. Using the new position vector (Eq. 26), the procedure is repeated until the error (Er) becomes smaller than the adopted tolerance (tol).

$$\vec{g}(\vec{Y_0}) = \frac{\partial \Pi}{\partial \vec{Y}}, \tag{24}$$

$$\Delta\vec{Y} = -(\mathbf{H})^{-1} \cdot \vec{g}(\vec{Y_0}), \tag{25}$$

$$\vec{Y} = \vec{Y_0} + \Delta\vec{Y}, \tag{26}$$

$$Er = \frac{|\Delta\vec{Y}|}{|\vec{X}|} \leq tol. \tag{27}$$

For conservative external forces, which is the assumption assumed herein, the Hessian matrix of the system is determined by deriving Eq. (20) regarding positions. In static analyses, where the kinetic energy is negligible, the static Hessian matrix $\mathbf{H}^{\text{est}}$ is given by:

$$H_{ij}^{\alpha\gamma(\text{est})} = \frac{\partial^2 \mathbb{U}}{\partial Y_i^{\alpha} \partial Y_j^{\gamma}} = \int_{V_0} h_{ij}^{\alpha\gamma} dV_0, \tag{28}$$

where:

$$h_{ij}^{\alpha\gamma} = \frac{\partial \mathbf{E}}{\partial Y_j^{\gamma}} : \frac{\partial \mathbf{S}}{\partial Y_i^{\alpha}} + \mathbf{S} : \frac{\partial^2 \mathbf{E}}{\partial Y_i^{\alpha} \partial Y_j^{\gamma}}. \tag{29}$$

For transient dynamic analyses, the numerical solution is performed by the Newmark temporal integrator (Newmark, 1959) together with the Newton-Raphson method. In Newmark's algorithm, time is a discrete parameter, whose current time instant (t_{s+1}) is the sum of the previous instant of time (t_s) and the time increment (or time step, Δt). Performing the second derivative of the total mechanical energy, the dynamic Hessian matrix $\mathbf{H}^{\text{din}}$ can be written as:

$$\mathbf{H}^{\text{din}} = \mathbf{H}^{\text{est}} + \frac{\partial^2 \mathbb{K}}{\partial Y_i^{\alpha} \partial Y_j^{\gamma}} = \mathbf{H}^{\text{est}} + \frac{1}{\beta \Delta t^2}\mathbf{M} + \frac{\gamma}{\beta \Delta t}\mathbf{C}, \tag{30}$$

in which $\mathbf{M}$ and $\mathbf{C}$ are the mass and viscous damping matrices, respectively, and β and γ are Newmark's constants. This study adopts $\beta = 1/4$ and $\gamma = 1/2$ in order to avoid spurious damping (Newmark, 1959).

After satisfying the stopping criterion (Eq. 27), the solution vector $\vec{Y}$ is used to recalculate the stress tensor $\mathbf{S}$ in order to post-process the Cauchy stress tensor ($\boldsymbol{\sigma}$), as follows:

$$\boldsymbol{\sigma} = \frac{\mathbf{A} \cdot \mathbf{S} \cdot \mathbf{A}^t}{\det(\mathbf{A})}. \tag{31}$$

It is worth mentioning that the stresses calculated by Eq. (31) are given along the transverse direction at the integration points (ξ_1, ξ_2, ξ_3). Thus, a Least Squares Technique is applied to interpolate the stress distribution to be written at element nodes. Regarding the stress representation along the thickness, these are computed directly at predefined points of the cross section.

3. NUMERICAL EXAMPLES

3.1 Dynamics of a tumbling cylinder

This first example seeks to validate the positional FEM formulation for large displacements. Therefore, we use the dynamic short cylinder problem, originally proposed by Simo and Tarnow (1994), and reproduced by Brank *et al.* (2003). The problem deals with an elastic ring, initially cylindrical, subjected to time-varying external forces $\vec{F}(t)$. The load is applied at symmetric positions along the height and spaced at 90° around its circumference. There are no restrictions of movements, i.e., the ring is free to move in any direction.

The cylinder has diameter D = 15.0, thickness h_0=0.02, and height 3.0 (compatible units). Its geometry was discretized using a mesh of 28x3 rectangles of same dimension, divided into two triangles (168 finite elements and 840 nodes), as depicted in Fig 1. The material is isotropic with the following properties: Young modulus E = 2.0x10^8, Poisson ratio ν = 0.5, and density ρ = 1.0.

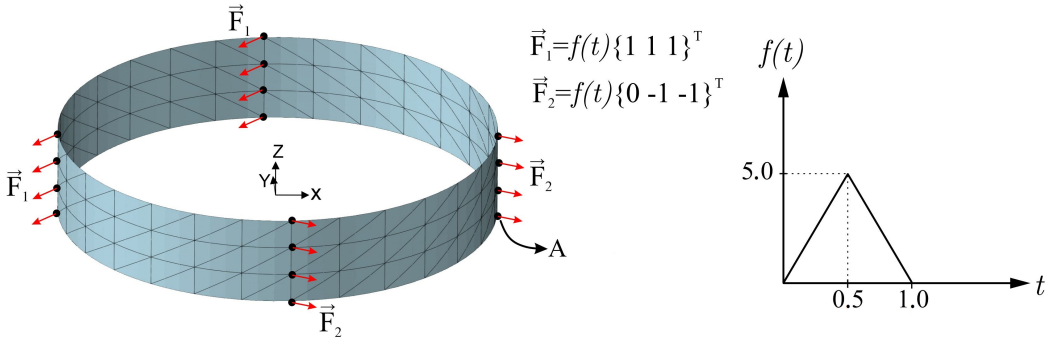

Figure 1. Geometry, discretization, and loading.

The time step (Δt) is equal to 0.01. As benchmark, we use a semi-analytical solution provided by Brank *et al.* (2003). These authors applied a mesh with 28x3 isoparametric four-node finite elements, and Newmark's time integration scheme (with β = 1/4, γ = 1/2 and Δt = 0.05). The displacement components at point A(D/2, 0, 0) are shown in Fig. 2.

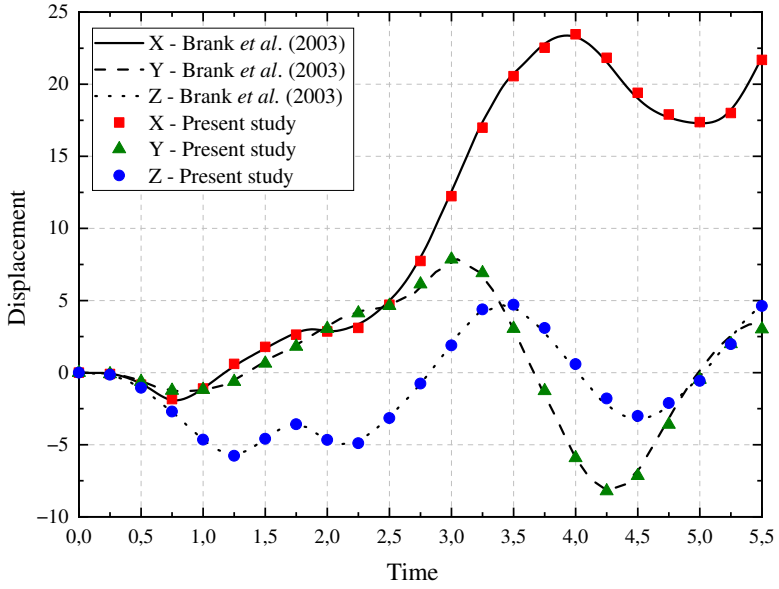

Figure 2. Displacement components at point A of the referente surface.

Good agreement between the results are provided for all three displacement components, indicating that the positional formulation is able to deal with large displacement analysis. As highlighted by Brank *et al.* (2003), the ring performs a complex free movement after the loadings ends (t = 1.0); depicted in Fig. 3. This movement remains continuously through time due to the lack of damping in the mechanical system.

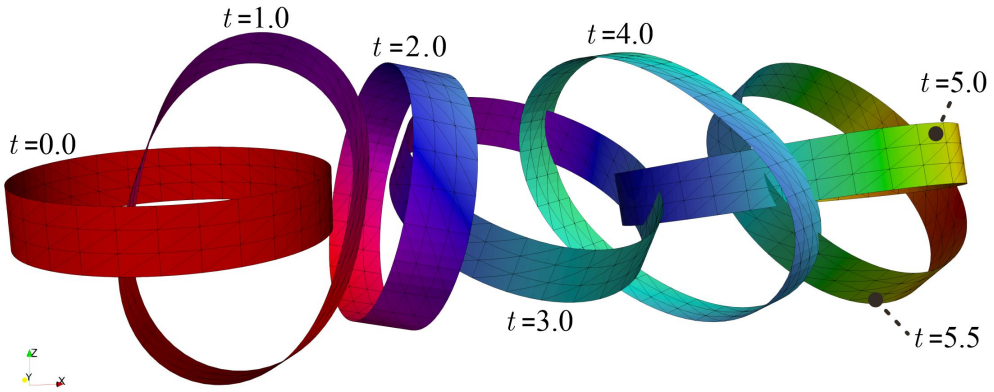

Figure 3. Ring displacement sequence in time interval [0; 5.5] (no scaling).

3.2 Laminated plate under harmonic load

This problem was solved analytically by Pagano (1969, 1970) and will be used here to validate the stress distribution in a laminated plate. As depicted in Fig. 4, the plate has dimensions $axbxh_0$ and is subjected to a transverse load on the upper surface $p(x, y) = q_0 sin(n\pi x/a)sin(m\pi y/b)$, with q_0 constant (maximum value of the load), n and m positive integers, and p positive in the $+z$-axis direction.

The ratio between length a and the height of the plate is given by $a/h_0 = S$, in which h_0 is divided into N layers of equal thickness. The layers have unidirectional fibers oriented at 0° or 90°, where 0° is the direction parallel to the x-axis and 90° the direction parallel to the y-axis.

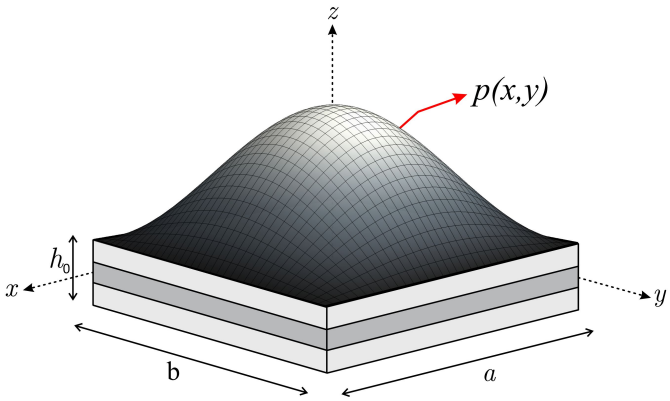

Figure 4. Laminated plate under harmonic load.

The material of the layers is orthotropic and simulates a composite following the given stiffness properties:

A) $E_1 = 25.0$ MPa, $E_2 = E_3 = 1.0$ MPa, $G_{12} = G_{13} = 0.50$ MPa, $G_{23} = 0.10$ MPa, $\nu_{12} = \nu_{13} = \nu_{23} = 0.25$;

B) $E_1 = 120.0$ MPa, $E_2 = 25$ MPa, $E_3 = 30.0$ MPa, $G_{12} = 0.40$ MPa, $G_{13} = 0.50$ MPa, $G_{23} = 0.30$ MPa, $\nu_{12} = 0.30$, $\nu_{13} = 0.25$, $\nu_{23} = 0.20$.

Table 1 presents the data of the simulated laminated composites, including geometry dimensions, material, cross-ply stacking sequence and finite element mesh discretization.

Table 1. Laminated composite cases.

Case	*a* (m)	*b* (m)	*n*	*m*	*N*	Material	Stacking	Mesh
L1	20.0	1.0	1	*	3	A	0°/90°/0°	(20x2)x2
L2	20.0	20.0	1	1	3	B	0°/90°/0°	(8x8)x2

$^* sin(m\pi y b^{-1}) = 1.0$

The plate is simply supported at the ends of length b in the L1 case, and simply supported at all edges in the L2 case. It is worth noting that the analytical solution developed by Pagano (1969) considers a state of plane strain with respect to the xy plane. To satisfy this assumption in the FEM analysis, the displacements in the y-axis direction are constrained for L1 case. In addition, to avoid quadratic variation of the thickness, the parameter T was prescribed equal zero throughout the mesh for all cases, in accordance with Pagano (1969, 1970). Furthermore, the displacements and stresses are computed as non-dimensional quantities, respectively, as follows:

$$\overline{u} = \frac{E_2 u}{q_0 h_0}, \tag{32}$$

$$\{\overline{\sigma}_x, \overline{\sigma}_y\} = \frac{h_0^2 \{\sigma_x, \sigma_y\}}{q_0 a^2}, \tag{33}$$

$$\{\overline{\tau}_{xz}, \overline{\tau}_{yz}\} = \frac{h_0 \{\tau_{xz}, \tau_{yz}\}}{q_0 a}. \tag{34}$$

The numerical solutions are identified by the acronyms RM-like for the basic kinematics, and ZZ-enriched for the enrichment with zigzag functions. The results are shown in Fig. 5, Fig. 6 and Fig. 7, respectively for L1 laminate, and Fig. 8 for L2 case.

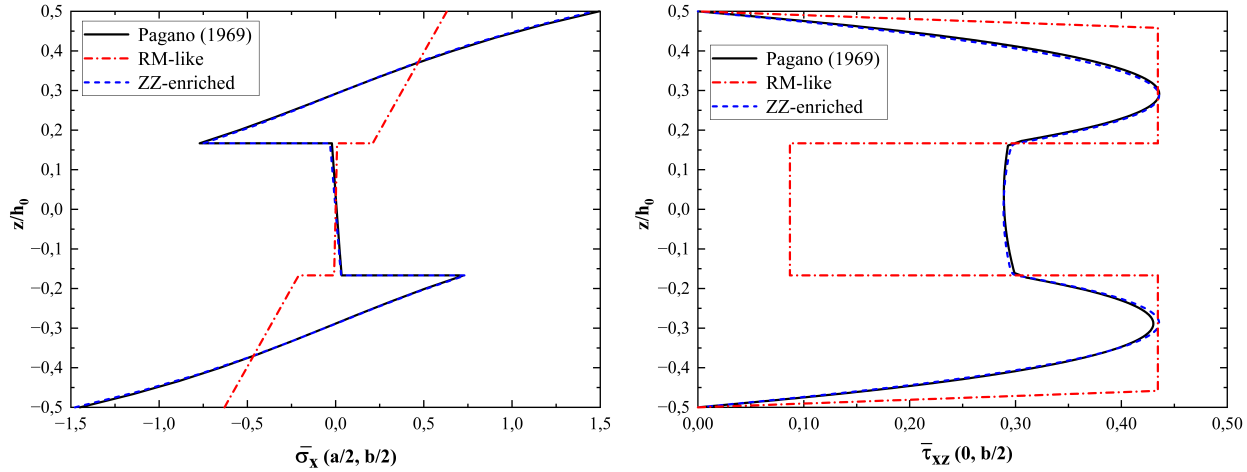

Figure 5. L1: dimensionless normal and shear stresses distribution ($S = 4$).

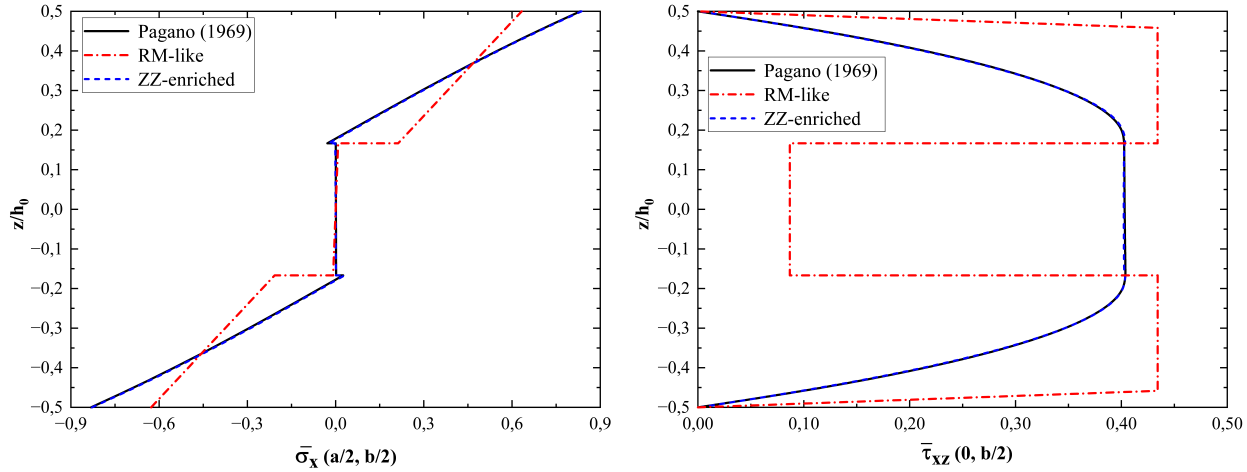

Figure 6. L1: dimensionless normal and shear stresses distribution ($S = 10$).

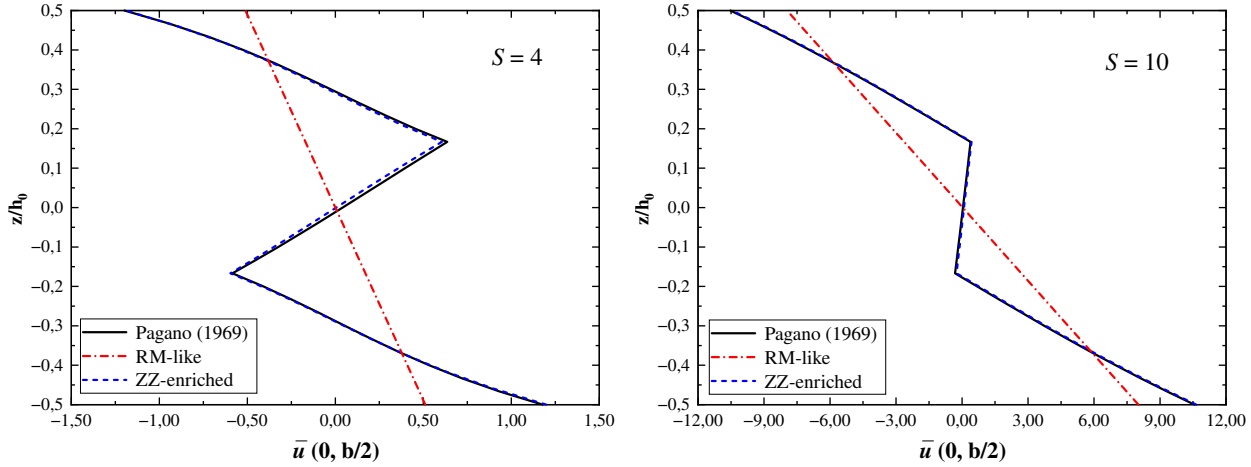

Figure 7. L1: dimensionless displacement in the x direction $vs.$ transverse position.

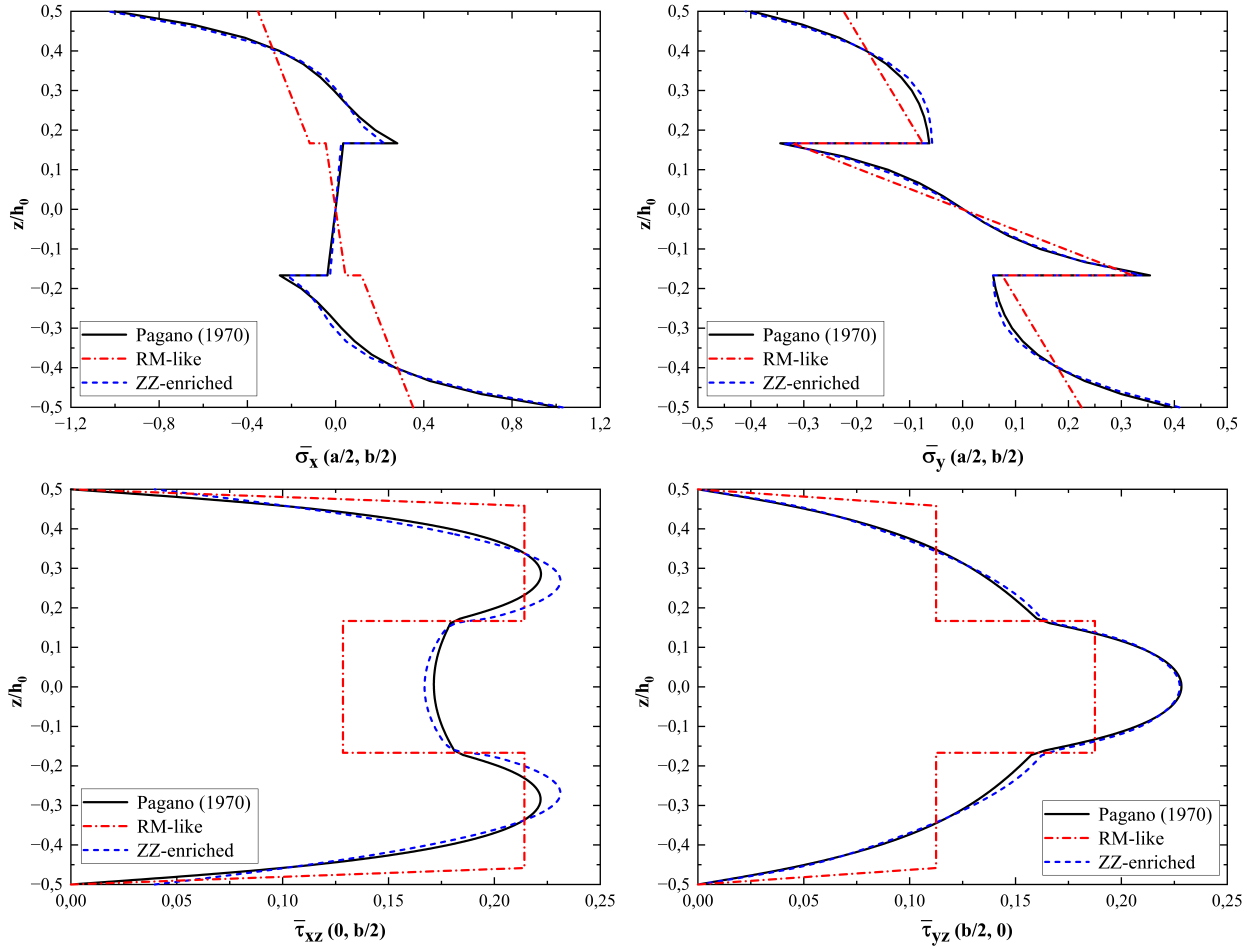

Figure 8. L2: dimensionless normal and shear stresses distribution ($S = 4$).

As demonstrated, for both thick ($S = 4$) and moderately thick ($S = 10$) laminates, the stress and displacement distributions through the thickness provided by the enriched formulation (ZZ-enriched) present good adherence regarding the analytical solutions of Pagano (1969, 1970). The same cannot be said for the Reissner-Mindlin-like kinematics (RM-like), which neglected the continuity of transverse shear stresses and the zigzag displacement. From Fig. 7, one observes that the zigzag pattern is more pronounced in thick laminated composites than moderately thick laminated. This result corroborates with the literature review (Reddy, 2004).

It is also worth noting that the results for the L1 case converges to the analytic solution almost exactly, while the L2 case presents a slightly deviation. We suspect that the reason is related to the influence of the strain in the in-plane displacements, since the L1 case assumes the assumption of plane state of strain. This supposition will be further investigated.

4. CONCLUSIONS

In this study we apply a positional description of the finite element method for geometric nonlinear analysis of plates and shells in static and dynamic problems. One example is presented and its results validate this formulation for transient dynamic problems developing large displacements. Furthermore, the transverse enrichment of the thickness ensured the kinematics free of volumetric locking. Regarding the distribution of transverse stresses and displacements in symmetrical laminates, the proposed kinematics is able to accurately simulate normal and shear stresses along the thickness, in addition to reproduce the zigzag pattern of displacement. The next developments aim to extend this formulation to asymmetric plate and shell laminates.

5. ACKNOWLEDGEMENTS

The authors acknowledge the Coordenação de Aperfeiçoamento de Pessoal de Nível Superior – Brasil (CAPES) – Grant Finance Code 001 – and the Conselho Nacional de Desenvolvimento Científico e Tecnológico (CNPq) for the financial support provided.

6. REFERENCES

Bischoff, M. and Ramm, E., 1997. "Shear deformable shell elements for large strains and rotations". *International Journal for Numerical Methods in Engineering*, Vol. 40, No. 23, pp. 4427–4449.

Bonet, J., Wood, R., Mahaney, J. and Heywood, P., 2000. "Finite element analysis of air supported membrane structures". *Computer methods in applied mechanics and engineering*, Vol. 190, No. 5-7, pp. 579–595.

Brank, B. *et al.*, 2003. "Dynamics and time-stepping schemes for elastic shells undergoing finite rotations". *Computers & structures*, Vol. 81, No. 12, pp. 1193–1210.

Carrera, E., 2003. "Historical review of zig-zag theories for multilayered plates and shells". *Appl. Mech. Rev.*, Vol. 56, No. 3, pp. 287–308.

Coda, H.B., 2018. *O Método dos Elementos Finitos Posicional: Sólidos e Estruturas – Não Linearidade Geométrica e Dinâmica*. EESC-USP, São Carlos, 1st edition. ISBN 978-85-8023-068-0.

Coda, H.B., 2003. "An exact FEM geometric non-linear analysis of frames based on position description". In *Proceedings of XVIII Congresso Brasileiro de Engenharia Mecânica (COBEM)*. São Paulo.

Coda, H.B., Bernardo, C.C.L.C.G. and Paccola, R.R., 2022. "A FEM formulation for the analysis of laminated and functionally graded hyperelastic beams with continuous transverse shear stresses". *Composite Structures*, Vol. 292, p. 115606.

Coda, H.B. and Paccola, R.R., 2007. "An alternative positional FEM formulation for geometrically non-linear analysis of shells: curved triangular isoparametric elements". *Computational Mechanics*, Vol. 40, No. 1, pp. 185–200.

Garg, A. and Chalak, H., 2019. "A review on analysis of laminated composite and sandwich structures under hygrothermal conditions". *Thin-Walled Structures*, Vol. 142, pp. 205–226.

Icardi, U., 2001. "A three-dimensional zig-zag theory for analysis of thick laminated beams". *Composite structures*, Vol. 52, No. 1, pp. 123–135.

Li, D., 2021. "Layerwise theories of laminated composite structures and their applications: a review". *Archives of Computational Methods in Engineering*, Vol. 28, No. 2, pp. 577–600.

Liew, K., Pan, Z. and Zhang, L., 2019. "An overview of layerwise theories for composite laminates and structures: Development, numerical implementation and application". *Composite Structures*, Vol. 216, pp. 240–259.

Newmark, N.M., 1959. "A method of computation for structural dynamics". *Journal of the engineering mechanics division*, Vol. 85, No. 3, pp. 67–94.

Pagano, N.J., 1970. "Exact solutions for rectangular bidirectional composites and sandwich plates". *Journal of composite materials*, Vol. 4, No. 1, pp. 20–34.

Pagano, N., 1969. "Exact solutions for composite laminates in cylindrical bending". *Journal of composite materials*, Vol. 3, No. 3, pp. 398–411.

Petrolo, M., Augello, R., Carrera, E., Scano, D. and Pagani, A., 2023. "Evaluation of transverse shear stresses in layered beams/plates/shells via stress recovery accounting for various cuf-based theories". *Composite Structures*, p. 116625.

Reddy, J.N., 2004. *Mechanics of laminated composite plates and shells: theory and analysis*. CRC press, Boca Raton, 2nd edition. ISBN 978-0849315923.

Simo, J.C. and Tarnow, N., 1994. "A new energy and momentum conserving algorithm for the non-linear dynamics of shells". *International Journal for Numerical Methods in Engineering*, Vol. 37, No. 15, pp. 2527–2549.

Soltani, Z. and Kordkheili, S.A.H., 2021. "Interlaminar stress analysis of composite shell structures using a geometrically nonlinear layer-wise shell finite element". *Composite Structures*, Vol. 257.

Sorrenti, M. and Gherlone, M., 2023. "A new mixed model based on the enhanced-refined zigzag theory for the analysis of thick multilayered composite plates". *Composite Structures*, Vol. 311, p. 116787.

Tessler, A., Di Sciuva, M. and Gherlone, M., 2009. "A refined zigzag beam theory for composite and sandwich beams". *Journal of Composite Materials*, Vol. 43, No. 9, pp. 1051–1081.

Tornabene, F., 2016. "General higher-order layer-wise theory for free vibrations of doubly-curved laminated composite shells and panels". *Mechanics of Advanced Materials and Structures*, Vol. 23, No. 9, pp. 1046–1067.

Vu-Quoc, L. and Tan, X., 2013. "Efficient hybrid-eas solid element for accurate stress prediction in thick laminated beams, plates, and shells". *Computer Methods in Applied Mechanics and Engineering*, Vol. 253, pp. 337–355.

Wanji, C. and Zhen, W., 2008. "A selective review on recent development of displacement-based laminated plate theories". *Recent patents on mechanical engineering*, Vol. 1, No. 1, pp. 29–44.

Wu, Y., Xing, Y. and Liu, B., 2018. "Analysis of isotropic and composite laminated plates and shells using a differential quadrature hierarchical finite element method". *Composite Structures*, Vol. 205, pp. 11–25.

7. RESPONSIBILITY NOTICE

The authors, V. B. Souza and H. B. Coda, are the only responsible for the printed material included in this paper.